Published OnlineFirst July 20, 2020; DOI: 10.1158/2159-8290.CD-20-0288

RESEARCH ARTICLE

Identification of BBOX1 as a Therapeutic Target in Triple-Negative Breast Cancer

Chengheng Liao[1], Yang Zhang[2], Cheng Fan[3], Laura E. Herring[4], Juan Liu[5], Jason W. Locasale[5], Mamoru Takada[6], Jin Zhou[1], Giada Zurlo[1], Lianxin Hu[1], Jeremy M. Simon[3,7,8], Travis S. Ptacek[3,8], Victor G. Andrianov[9], Einars Loza[9], Yan Peng[1], Huanghe Yang[2], Charles M. Perou[3], and Qing Zhang[1]

Published OnlineFirst July 20, 2020; DOI: 10.1158/2159-8290.CD-20-0288

ABSTRACT Triple-negative breast cancer (TNBC) is an aggressive and highly lethal disease. Because of its heterogeneity and lack of hormone receptors or HER2 expression, targeted therapy is limited. Here, by performing a functional siRNA screening for 2-OG–dependent enzymes, we identified gamma-butyrobetaine hydroxylase 1 (*BBOX1*) as an essential gene for TNBC tumorigenesis. BBOX1 depletion inhibits TNBC cell growth while not affecting normal breast cells. Mechanistically, BBOX1 binds with the calcium channel inositol-1,4,5-trisphosphate receptor type 3 (IP3R3) in an enzymatic-dependent manner and prevents its ubiquitination and proteasomal degradation. BBOX1 depletion suppresses IP3R3-mediated endoplasmic reticulum calcium release, therefore impairing calcium-dependent energy-generating processes including mitochondrial respiration and mTORC1-mediated glycolysis, which leads to apoptosis and impaired cell-cycle progression in TNBC cells. Therapeutically, genetic depletion or pharmacologic inhibition of BBOX1 inhibits TNBC tumor growth *in vitro* and *in vivo*. Our study highlights the importance of targeting the previously uncharacterized BBOX1–IP3R3–calcium oncogenic signaling axis in TNBC.

SIGNIFICANCE: We provide evidence from unbiased screens that BBOX1 is a potential therapeutic target in TNBC and that genetic knockdown or pharmacologic inhibition of BBOX1 leads to decreased TNBC cell fitness. This study lays the foundation for developing effective BBOX1 inhibitors for treatment of this lethal disease.

INTRODUCTION

Triple-negative breast cancer (TNBC) is a highly heterogeneous and clinically aggressive disease that accounts for 15% to 20% of breast cancers, causing the highest mortality rate among all breast cancer subtypes (1, 2). TNBC is an IHC-defined subtype of breast cancer that does not express estrogen receptor (ER) or progesterone receptor (PR), and lacks human *HER2* amplification. In contrast to hormone receptor–positive breast cancer, which is commonly treated with endocrine therapy, or HER2-positive breast cancer that can be treated by therapeutic antibodies (e.g., trastuzumab), TNBC has no effective targeted therapy, and conventional chemotherapy remains the standard of care for patients with TNBC (3). Therefore, the identification of novel targets with actionable therapeutic drugs that specifically target TNBC vulnerabilities could greatly benefit the clinical outcome of patients with TNBC.

2-oxoglutarate (2-OG)-dependent enzymes, which use oxygen and 2-OG as cosubstrates and Fe(II) as a cofactor, catalyze various cellular biological enzymatic reactions with a broad spectrum of substrates (e.g., DNA, RNA, and proteins; ref. 4). Emerging literature indicates that they also play important roles in various malignant diseases. For example, the function of TET DNA hydroxylases has been well documented in hematologic malignancies (4). Prolyl hydroxylases regulate cancer cell growth by modulating the level of their substrates, including hypoxia-inducible factors alpha (HIFα) and forkhead box O3A (FOXO3A; refs. 5, 6). Histone demethylases, by modulating methylation of some histone residues including H3K4 and H3K36, regulate gene expression that has been linked to the pathogenesis of several cancers (7, 8). Our recent studies suggested that the hydroxylase EGLN2 and its downstream substrate adenylosuccinate lyase (ADSL) positively contribute to TNBC tumorigenesis (9, 10). These studies indicate that the dysfunction of 2-OG–dependent enzymes may associate with various cancers including breast cancer. However, we lack a systematic approach to unbiasedly screen for critical enzymes that contribute to TNBC progression.

In this study, we sought to identify novel therapeutic targets in TNBC among 2-OG–dependent enzymes through an unbiased siRNA library screening, with the gene depletion affecting cell growth in both two-dimensional (2-D) cell proliferation and three-dimensional (3-D) anchorage-independent growth. We show that gamma-butyrobetaine hydroxylase 1 (BBOX1), a member of the 2-OG–dependent enzymes catalyzing carnitine biosynthesis (11) that has never been characterized in cancers, is important for TNBC progression. We aim to characterize the oncogenic function of BBOX1, elucidate the molecular

[1]Department of Pathology, The University of Texas Southwestern Medical Center, Dallas, Texas. [2]Department of Biochemistry, Duke University, Durham, North Carolina. [3]Lineberger Comprehensive Cancer Center, University of North Carolina School of Medicine, Chapel Hill, North Carolina. [4]Department of Pharmacology and UNC Proteomics Core Facility, University of North Carolina, Chapel Hill, North Carolina. [5]Department of Pharmacology and Cancer Biology, Duke University School of Medicine, Durham, North Carolina. [6]Department of General Surgery, Chiba University Graduate School of Medicine, Chiba, Japan. [7]Department of Genetics, Neuroscience Center, University of North Carolina, Chapel Hill, North Carolina. [8]UNC Neuroscience Center, Carolina Institute for Developmental Disabilities, University of North Carolina, Chapel Hill, North Carolina. [9]Latvian Institute of Organic Synthesis, Riga, Latvia.

Note: Supplementary data for this article are available at Cancer Discovery Online (http://cancerdiscovery.aacrjournals.org/).

Corresponding Author: Qing Zhang, UT Southwestern Medical Center, 5323 Harry Hines Boulevard, NB7.208, Dallas, TX 75390-9072. Phone: 214-645-4671; Fax: 214-648-1102; E-mail: Qing.Zhang@UTSouthwestern.edu

Cancer Discov 2020;10:1–16

doi: 10.1158/2159-8290.CD-20-0288

Published OnlineFirst July 20, 2020; DOI: 10.1158/2159-8290.CD-20-0288

mechanism by which BBOX1 contributes to TNBC, and explore its therapeutic potential in relevant TNBC models.

RESULTS

Identification of BBOX1 as an Essential Gene for TNBC Cell Growth

To identify potential 2-OG–dependent enzymes that may contribute to TNBC cell growth, we obtained an on-target plus siRNA library that targets all the members of this family of enzymes (Supplementary Table S1). We developed a screening method that examines both 2-D MTS cell proliferation and 3-D anchorage-independent growth with a representative TNBC cell line, MDA-MB-231 (Supplementary Fig. S1A). In addition, we included several independent siRNAs for the housekeeping gene *GAPDH*, which scored among the top hits from the screening (Fig. 1A). We identified nine enzymes that scored in both the 2-D and 3-D screening, showing significant growth defect upon gene depletion by siRNAs (Fig. 1B and C; Supplementary Fig. S1B). Among them, jumonji domain-containing protein 6 (JMJD6) and lysine demethylase 6A (KDM6A) have been previously identified to be important for maintaining MDA-MB-231 cell growth (12, 13). Among other positive hits from our screening, AlkB homolog 4 lysine demethylase (ALKBH4) depletion led to decreased cell proliferation in MDA-MB-231 cells, but also in the immortalized normal breast epithelial cell line HMLE (Supplementary Fig. S1C and S1D), suggesting that ALKBH4 may be an essential gene for both normal cell and breast cancer cell survival. Interestingly, two enzymes involved in carnitine synthesis, BBOX1 and trimethyllysine hydroxylase epsilon (TMLHE), were found to be critical for TNBC cell growth, suggesting the importance of this pathway in TNBC. We tested either BBOX1/TMLHE deletion alone or in combination in MDA-MB-231 cells and found no significant additive effect on cell proliferation or soft-agar growth with codeletion compared with either gene deletion (Supplementary Fig. S1E–S1H). Because BBOX1 acts downstream of TMLHE in the carnitine synthesis pathway, we decided to focus on the characterization of BBOX1 in TNBC. Indeed, BBOX1 was found to be essential for the growth of multiple TNBC cells (MDA-MB-231, 436, and 468; Fig. 1D and E; Supplementary Fig. S1I) but not for the normal breast epithelial cell line as verified by two individual siRNAs (Supplementary Fig. S1J–S1L).

Our screening data suggest that BBOX1 may be an oncogene in TNBC. We examined BBOX1 protein levels in a panel of breast cancer cell lines and found that BBOX1 expression was generally higher in basal-like breast cancer cell lines compared with other subtypes of breast cancer cells or normal breast epithelial cells (Fig. 1F). In the breast cancer patient datasets The Cancer Genome Atlas (TCGA), METABRIC, and UNC337 (14–16), BBOX1 expression was the highest in patients with basal-like breast cancer, which includes most patients with TNBC (ref. 17; Fig. 1G). In addition, higher expression of BBOX1 predicted worse prognosis only in patients with basal-like TNBC, but not in patients with luminal A, luminal B, or HER2$^+$ breast cancer (Fig. 1H).

In line with the results obtained with siRNAs, BBOX1 depletion by shRNAs induced a growth-deficient phenotype in both 2-D MTS assay and colony formation, as well as 3-D soft agar in TNBC cells, including MDA-MB-468, HCC70, and HCC3153 (Fig. 2A–C; Supplementary Fig. S2A). BBOX1 depletion in BT474, a BBOX1-high expressing HER2$^+$ cell line (Fig. 1F), also caused a similar growth defect phenomenon (Fig. 2A–C; Supplementary Fig. S2A). However, BBOX1 depletion in the BBOX1-low expressing breast cancer cell lines (MCF-7 and T47D) or normal breast epithelial cell lines (MCF-10A and HMLE) did not cause an overt effect on cell proliferation (Fig. 2A–C; Supplementary Fig. S2B). Collectively, these data show that BBOX1 depletion caused a cell proliferation defect preferentially in TNBC cells. However, its knockdown could also lead to growth defects in other subtypes of breast cancer cells displaying high BBOX1 protein levels.

BBOX1 Promotes TNBC Cell Growth in an Enzymatic-Dependent Fashion

Next, we aimed to examine whether BBOX1 overexpression induces TNBC cell proliferation and, if so, whether this phenotype is mediated by its enzymatic activity. First, we found that overexpression of BBOX1 promotes the 2-D or 3-D cell growth in MDA-MB-436, SUM149, MCF-10A, and HMLE (Supplementary Fig. S2C–S2G). We then infected MDA-MB-231, 436, and 468 cells with vector, wild-type (WT), or catalytically inactive mutant (N2D) BBOX1 by double-mutating the two key amino acid residues (Asn191, Asn292) which are critical for substrate γ-butyrobetaine (GBB) binding (18). In these cell lines, we observed increased cell proliferation with WT BBOX1 overexpression, and this phenotype was not observed with BBOX1-N2D–mutant expression despite the fact that WT and N2D BBOX1 had similar expression (Fig. 2D and E; Supplementary Fig. S2H–S2K). Next, we depleted endogenous BBOX1 from MDA-MB-468 cells followed by the restoration of either shRNA-resistant WT BBOX1 or BBOX1-N2D (Fig. 2F). WT BBOX1, but not BBOX1-N2D, efficiently rescued the defects in cell proliferation, 2-D colony growth, and 3-D soft-agar growth induced by BBOX1 depletion in these cells (Fig. 2G–I). Our results suggest that BBOX1 promotes TNBC cell growth in an enzymatic-dependent manner.

BBOX1 is a critical enzyme involved in carnitine synthesis (19). Carnitine is essential for lipid metabolism by transporting long-chain fatty acids into the mitochondria for β-oxidation (20). We asked whether BBOX1 regulates TNBC cell growth through carnitine synthesis. To this end, we performed a metabolomics study in MDA-MB-468 cells. More than 300 metabolites were detected in these cells with approximately 130 metabolites that were decreased ($P < 0.05$) in BBOX1 knockdown (KD) cells (Fig. 2J). We then conducted metabolic pathway analysis (21) and found that BBOX1 depletion affected the carnitine synthesis pathway (Fig. 2K), which was also confirmed by a modest but statistically significant decrease in carnitine level upon BBOX1 KD in TNBC cells (Fig. 2L). To examine the function of carnitine in TNBC cells, we supplied the MDA-MB-468 shRNA control or BBOX1 KD cells with carnitine and palmitate in fatty acid–free conditioned medium and measured the mitochondrial oxygen consumption rate (OCR) as an indicator of exogenous fatty acid oxidation (FAO). Indeed, carnitine supplementation had an effect on utilization of palmitate to promote OCR in MDA-MB-468 cells (Supplementary Fig. S2L). However, we found that the FAO-based OCR rate in BBOX1 KD cells was still lower than the control cells (Fig. 2M), indicating that carnitine is not sufficient to

Published OnlineFirst July 20, 2020; DOI: 10.1158/2159-8290.CD-20-0288

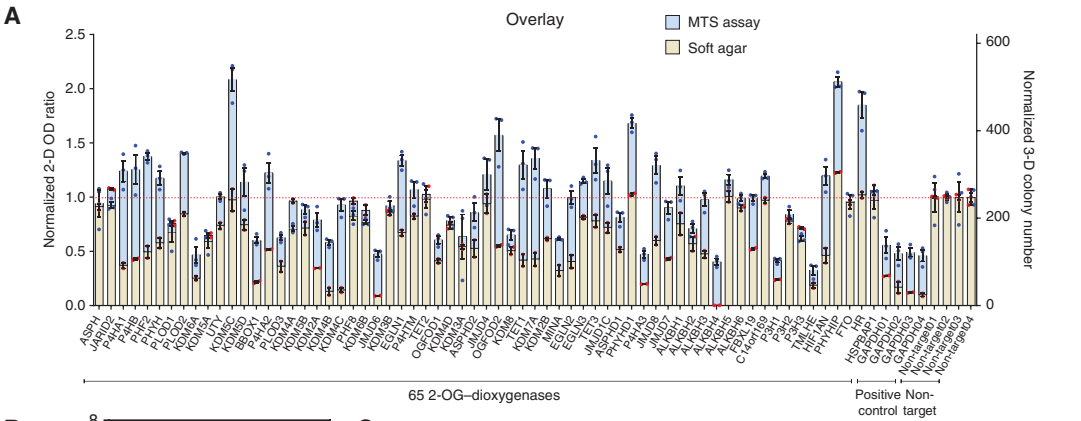

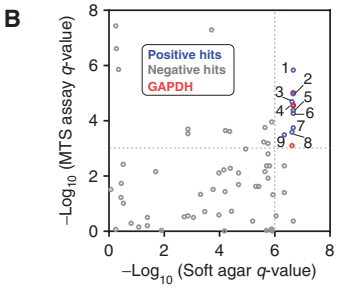

C

No.	Positive hits	MTS assay *q*-value	Soft agar *q*-value	siRNA effect on MTS growth	siRNA effect on soft-agar growth
1	TMLHE	1.44E-06	2.14E-07	Decrease	Decrease
2	KDM6A	1.05E-05	2.14E-07	Decrease	Decrease
3	P3H1	2.03E-05	2.33E-07	Decrease	Decrease
4	ALKBH4	2.67E-05	2.14E-07	Decrease	Decrease
5	P4HA3	4.13E-05	2.14E-07	Decrease	Decrease
6	JMJD6	5.34E-05	2.14E-07	Decrease	Decrease
7	BBOX1	1.77E-04	2.14E-07	Decrease	Decrease
8	KDM4B	2.56E-04	2.35E-07	Decrease	Decrease
9	MINA	3.21E-04	4.46E-07	Decrease	Decrease

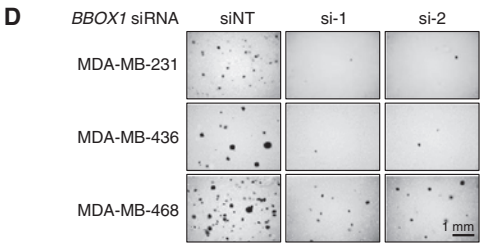

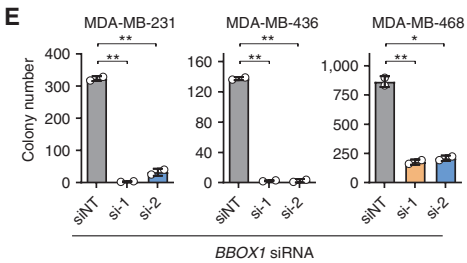

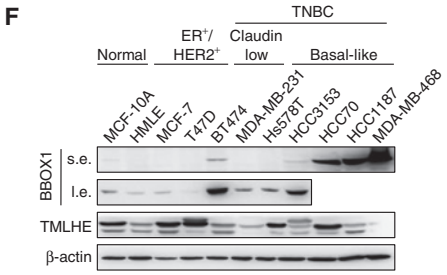

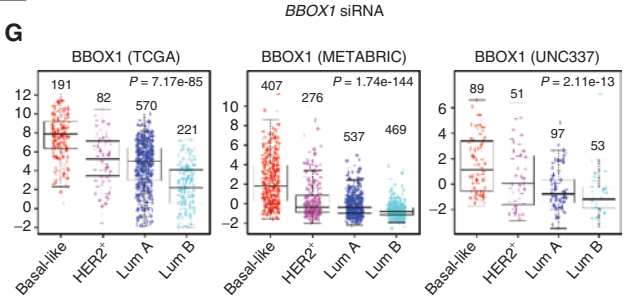

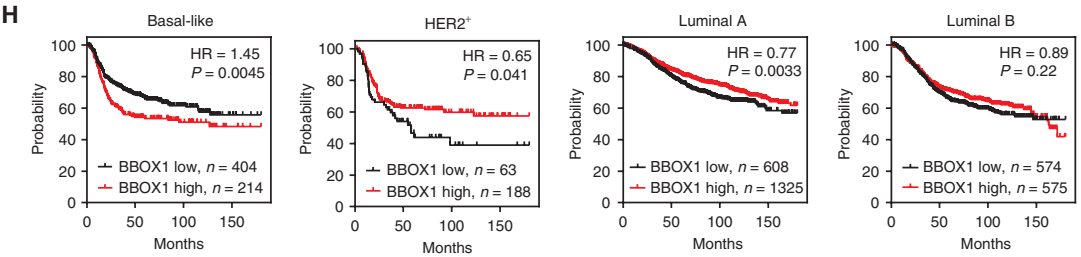

Figure 1. BBOX1 is required for TNBC cell growth. **A,** Overlay of MTS assay and soft-agar results for the screening. GAPDH was used as a positive control for the siRNA library screening. **B,** Dot plot shows the genes scored both in the MTS assay and in the soft-agar screening. $q < 0.001$ (MTS assay) and $q < 0.000001$ (soft agar) were used as cutoff. **C,** Lists of genes identified as significantly changing growth in MTS assay and soft-agar assay of MDA-MB-231 cells. **D,** Soft-agar colony growth of TNBC cells (MDA-MB-231, 436, 468) transfected with nontargeting (NT) siRNA control or two individual *BBOX1* siRNAs. **E,** Quantification of the soft-agar colony number related to **D**. Error bars, SEM, two-tailed Student *t* test (*, $P < 0.05$; **, $P < 0.01$). **F,** Immunoblot of endogenous BBOX1 and TMLHE protein levels in a panel of normal breast epithelial cell lines and breast cancer cell lines. s.e., short exposure time; l.e., long exposure time. **G,** *BBOX1* mRNA expression across different subtypes of breast cancer in the TCGA, METABRIC, and UNC337 datasets. Sample numbers are shown above each subtype. **H,** Kaplan–Meier plots of survival data for patients with breast cancer with intrinsic subtypes stratified by *BBOX1* mRNA expression levels. Patient numbers are shown.

Published OnlineFirst July 20, 2020; DOI: 10.1158/2159-8290.CD-20-0288

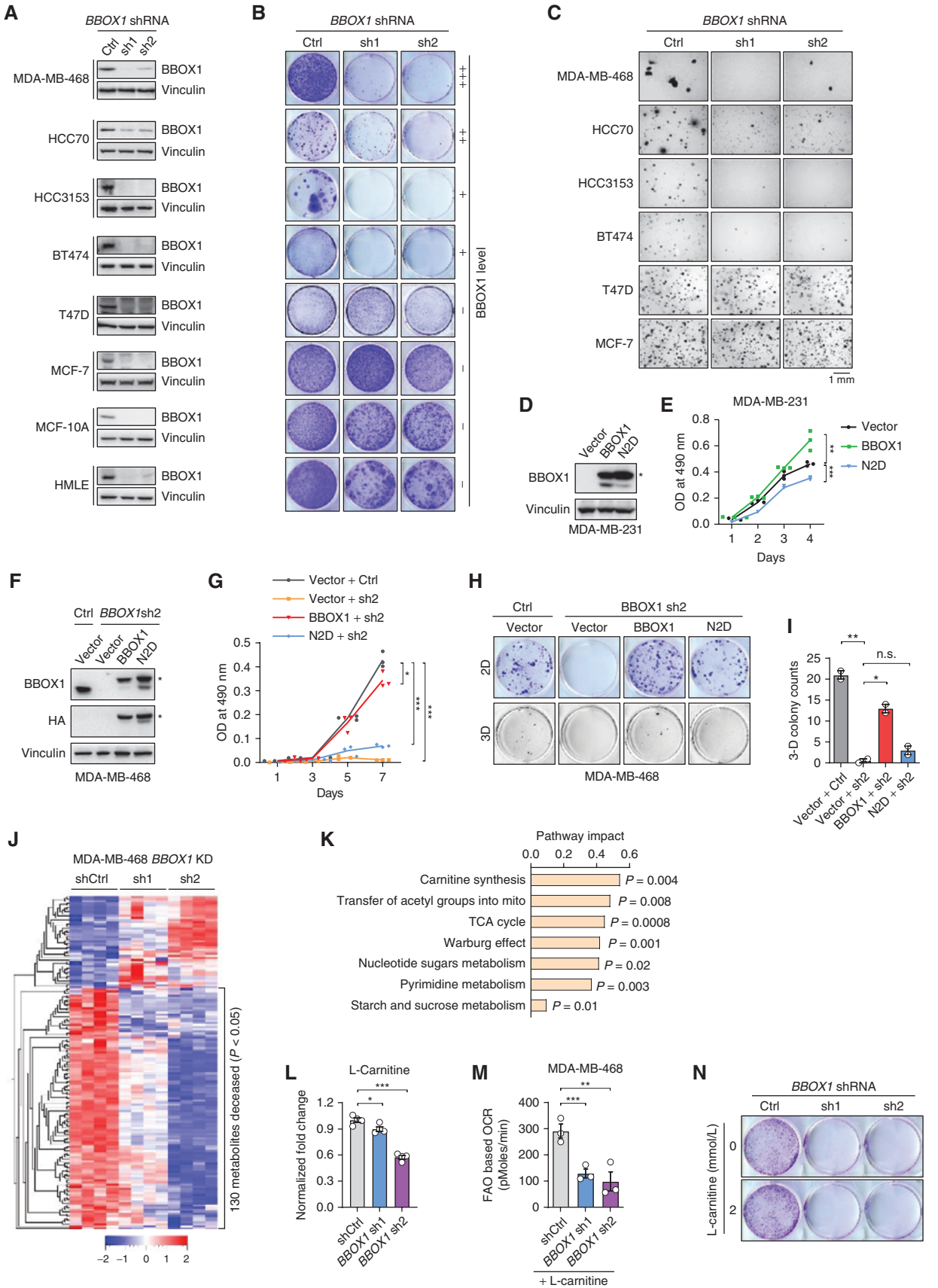

Published OnlineFirst July 20, 2020; DOI: 10.1158/2159-8290.CD-20-0288

rescue the defect of OCR in BBOX1 KD cells. In addition, the carnitine supplement failed to rescue the growth defect of MDA-MB-468 BBOX1-depleted cells (Fig. 2N). Collectively, these data show that BBOX1 promotes TNBC cell growth via its catalytic activity but independent of carnitine biosynthesis.

BBOX1 Controls IP3R3 Protein Stability in TNBC

To understand the potential molecular mechanism of BBOX1-positive regulation of TNBC cell proliferation, we performed TAP-TAG purification followed by mass spectrometry in MDA-MB-231 cells expressing either empty vector (EV), WT, or N2D BBOX1 to identify the BBOX1-binding proteins in each of these conditions (Fig. 3A). Whereas an equal number of BBOX1 peptides were retrieved from both WT and catalytically dead N2D, inositol 1,4,5-trisphosphate receptor type 3 (*ITPR3*, also known as IP3R3) was the top hit with the most peptides detected in the WT BBOX1, but not in the EV- or BBOX1-N2D–expressing cells (Fig. 3B), suggesting that IP3R3 is a unique BBOX1-binding partner and its binding depends on BBOX1 enzymatic activity. IP3R3 is an important endoplasmic reticulum (ER) calcium channel protein for the control of intracellular calcium release from the ER into the mitochondria (22). Emerging literature has highlighted IP3R3 as the specific protein among the three close family members (IP3R1, IP3R2, and IP3R3) contributing to malignancy in multiple cancers, including breast cancer (23–26). Coimmunoprecipitations (co-IP) in multiple TNBC cell lines further confirmed the binding of IP3R3 to WT BBOX1, but not catalytically deficient N2D mutant BBOX1 (Fig. 3C; Supplementary Fig. S3A and S3B). Importantly, we also observed this interaction in a physiologic setting, showing that the endogenous BBOX1 could bind with endogenous IP3R3 in TNBC cell lines including HCC70 and MDA-MB-468 (Fig. 3D; Supplementary Fig. S3C).

IP3R3 encodes a protein that harbors 2,671 amino acids, which makes the expression of full-length constructs challenging. To investigate the potential domain on IP3R3 that may bind with BBOX1, we obtained a series of IP3R3 truncation mutants (1–226 aa, 227–800 aa, 801–2230 aa, and 2,180–2,670 aa), as published previously (Supplementary Fig. S3D; ref. 27), and found that the amino acid sequence spanning from 227 to 800 was the major domain responsible for binding with BBOX1 (Supplementary Fig. S3E). We also obtained two additional truncation mutants (232–436 and 436–587 aa) and found that the region containing 232–436 amino acids bound to BBOX1 (Supplementary Fig. S3F).

Previous research showed that the IP3R3 amino acid sequence between 227 and 602 was mainly responsible for its binding with the E3 ubiquitin ligase F-box and leucine-rich repeat protein 2 (FBXL2) followed by its ubiquitination and degradation (27). Interestingly, in our system, we found that FBXL2 interacts with the IP3R3 region located between amino acids 232–587, which covers the same region bound by BBOX1 (Supplementary Fig. S3G). Therefore, we speculated that BBOX1 might bind with IP3R3 and affect its protein stability. To test this, we first examined the protein levels of IP3R3 upon BBOX1 knockdown in multiple TNBC cell lines. BBOX1 depletion mediated by shRNAs led to decreased IP3R3 protein level in these cell lines, while leaving the other two homologs, IP3R1 and IP3R2, unaffected (Fig. 3E). In support of this finding, doxycycline-induced BBOX1 depletion also led to decreased IP3R3 protein levels (Fig. 3F). This phenotype could be rescued by cotreatment of these BBOX1-depleted cells with the proteasomal inhibitor MG132 or the neddylation inhibitor MLN4924 (ref. 28; Fig. 3G; Supplementary Fig. S4A), suggesting that IP3R3 is subjected to ubiquitin-mediated proteasomal degradation and its protein stability is regulated by BBOX1. Consistently, BBOX1 depletion led to increased IP3R3 ubiquitination, which corresponded to decreased IP3R3 protein levels in these cells (Fig. 3H). We also performed pulse-chase experiments with cycloheximide to inhibit new protein synthesis and found that BBOX1 depletion led to decreased IP3R3 protein stability (Fig. 3I; Supplementary Fig. S4B and S4C). Because IP3R3 protein was previously shown to be degraded by FBXL2 E3 ligase (27), and we recapitulated the phenomenon in TNBC cells (Fig. 3J), we aimed to determine whether BBOX1 might affect the binding between FBXL2 and IP3R3. First, we overexpressed different dosages of BBOX1 and found that increased WT, but not catalytically dead, BBOX1 expression correlated with decreased binding of FBXL2 and IP3R3, corresponding with decreased IP3R3 ubiquitination (Fig. 3K and L; Supplementary Fig. S4D). In accordance with this finding, WT BBOX1, but not BBOX1-N2D, rescued the protein levels of IP3R3 regulated by BBOX1 depletion by both shRNAs (Fig. 3M; Supplementary Fig. S4E). Overexpression of the WT BBOX1, but not the N2D mutant, increased IP3R3 protein level in multiple breast cancer cell lines or normal epithelial cells (Supplementary Fig. S4F). In accordance with the regulation of IP3R3 by BBOX1, IP3R3 and BBOX1 protein levels also showed similar expression patterns in these basal-like TNBC cells (Fig. 3N). Interestingly, BBOX1 and IP3R3 protein levels did not correlate well in claudin-low MDA-MB-231 cells (Fig. 3N), which suggests other layers of regulation of IP3R3 exist in this cell line, such as PTEN, as published previously (27). To further examine the clinical relevance of BBOX1 expression in patients with breast

Figure 2. BBOX1 promotes TNBC cell growth in an enzymatically dependent fashion. **A–C,** Immunoblot analysis (**A**), 2-D colony formation assay (**B**), and representative soft-agar images (**C**) of indicated BBOX1-depleted breast cancer cells or normal epithelial cells. BBOX1 expression level of cells was indicated according to Fig. 1F. **D** and **E,** Immunoblot analysis (**D**) and MTS cell proliferation (**E**) of MDA-MB-231 stable cell lines expressing control vector (Vector), FLAG-3 × HA tagged wild-type BBOX1 (BBOX1) or N2D mutant (N2D). **F–I,** Immunoblot analysis (**F**), MTS cell proliferation (**G**), 2-D colony formation (top) and 3-D soft agar (bottom; **H**), and quantification of soft-agar colonies (**I**) of MDA-MB-468 stable cell lines expressing control vector (Vector), FLAG-3 × HA tagged wild-type BBOX1 (BBOX1) or N2D mutant (N2D) followed by infection with the indicated shRNA. **J,** Unbiased hierarchical clustering of significantly changed ($P < 0.05$) metabolite abundances in MDA-MB-468 BBOX1 KD or control cells. **K,** Pathway analysis of the significantly decreased metabolites in BBOX1-depleted cells showing the top seven enriched metabolic pathways. **L,** Normalized fold change of carnitine level in MDA-MB-468 BBOX1 knockdown or control cells. **M,** FAO-based OCR measurement in MDA-MB-468 BBOX1 knockdown or control cells supplemented with 1 mmol/L L-carnitine. **N,** Colony formation of carnitine rescue experiments. Control or BBOX1-depleted MDA-MB-468 cells were supplemented with 2 mmol/L L-carnitine. All error bars represent SEM, two-tailed Student *t* test (*, $P < 0.05$; **, $P < 0.01$; ***, $P < 0.001$; n.s., denotes no significance; * in **D** and **F** indicates exogenous BBOX1 proteins).

Published OnlineFirst July 20, 2020; DOI: 10.1158/2159-8290.CD-20-0288

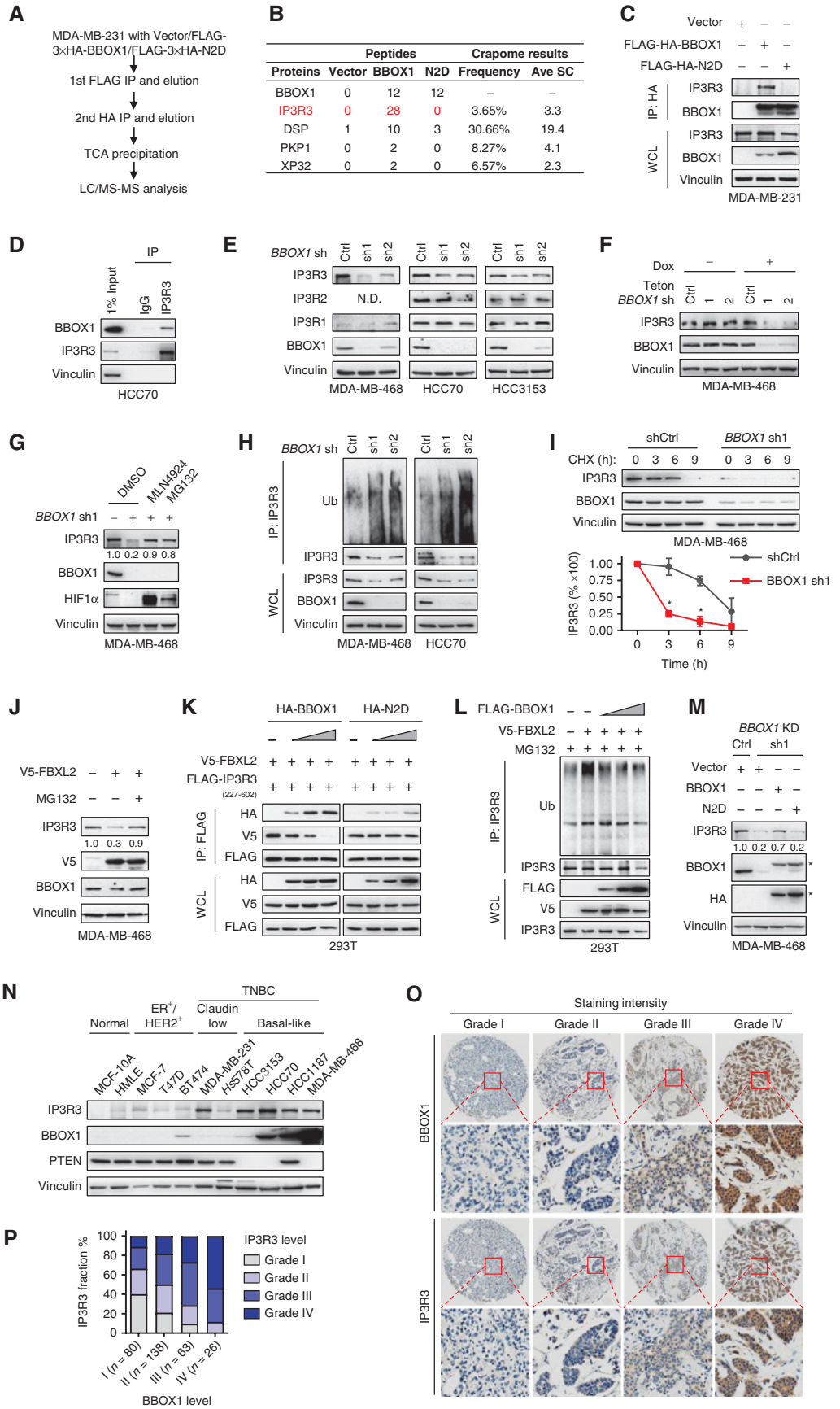

Published OnlineFirst July 20, 2020; DOI: 10.1158/2159-8290.CD-20-0288

cancer, we stained two different commercially available breast cancer tissue microarray (TMA) sets containing all breast cancer subtypes with BBOX1 as well as IP3R3, followed by the quantification of signal intensities. H score was used to determine the IHC staining intensities with these two proteins and was divided into four grades (I–IV) based on the staining intensity (29). IP3R3 protein expression level correlated strongly with BBOX1 in these breast cancer TMAs (Fig. 3O and P; Supplementary Fig. S4G and S4H), suggesting the clinical relevance of BBOX1–IP3R3 in patients with breast cancer. In conclusion, our results show that BBOX1 binds IP3R3 in an enzymatic-dependent manner and protects IP3R3 from FBXL2-mediated ubiquitination and degradation.

BBOX1–IP3R3–Calcium Signaling Sustains Mitochondrial Activity and mTORC1-Dependent Glycolysis That Is Required for TNBC Cell Growth and Survival

Next, we sought to examine the biological function of BBOX1-mediated IP3R3 regulation in TNBC cells. A previous study reported that constitutive IP3R3-mediated calcium release is required for maintaining cellular bioenergetics, contributing to sustained mitochondrial function and eventually cell proliferation (30). Because BBOX1 depletion led to decreased IP3R3 protein levels (Fig. 3E and F), we first examined the effect of BBOX1 on ER calcium release. We found that the ATP-induced intracellular calcium elevation in TNBC cells was mainly obtained through IP3R3-mediated ER calcium release because (i) calcium influx through the plasma membrane was prevented by the absence of extracellular calcium, and (ii) knockdown of IP3R3 essentially eliminated ATP-induced calcium responses (refs. 27, 31; Fig. 4A). Notably, ATP-induced ER calcium release was significantly reduced when knocking down BBOX1 compared with the control (Fig. 4A; Supplementary Fig. S5A). Next, we investigated whether BBOX1-mediated calcium release could affect mitochondrial function. We first showed that in MDA-MB-468 and HCC70 but not MCF-10A cells, depletion of IP3R3 significantly decreased OCR as an indication of mitochondrial activity (Fig. 4B and C; Supplementary Fig. S5B and S5C), which is consistent with the previous report (30). BBOX1 depletion also led to decreased OCR in MDA-MB-468 and HCC70 cells (Fig. 4D), and the phenotype was rescued by WT but not the N2D catalytic mutant BBOX1 (Supplementary Fig. S5D and S5E). Moreover, the metabolomics pathway analysis (Fig. 2K) showed that the tricarboxylic acid (TCA) cycle–related metabolites, such as citrate, ATP, and NADH, decreased upon BBOX1 depletion (Fig. 4E; Supplementary Fig. S5F). Despite comparable BBOX1 knockdown with two hairpins, metabolomics showed that *BBOX1* sh2 displayed more robust effect than sh1, which remains to be investigated.

Interestingly, besides the TCA cycle, we observed that some other important metabolic pathways were also enriched in the metabolomics analysis, such as the Warburg effect (aerobic glycolysis) and pyrimidine metabolism (Fig. 2K), which are frequently altered or reprogrammed in cancer cells (32, 33). The glycolysis pathway was also suppressed, with decreased glycolytic metabolites and increased glucose (Supplementary Fig. S5F and S5G). To understand how BBOX1 depletion may affect the metabolic changes we observed, we performed BBOX1 gene expression profiling by RNA sequencing (RNA-seq), and gene set enrichment analysis (GSEA) showed that the glycolysis pathway was enriched in control cells compared with BBOX1-depleted MDA-MB-468 cells (Fig. 4F and G; Supplementary Fig. S6A). Interestingly, we also noted that the mTORC1 pathway, a key regulator of glycolysis in cancer cells (34, 35), was enriched in our GSEA (Fig. 4F and G; Supplementary Fig. S6B), suggesting the suppression of mTORC1 might account for the impaired glycolysis in BBOX1 KD cells.

Next, we sought to address how mTORC1 is affected upon BBOX1 depletion. Notably, there is emerging literature indicating that cytosolic calcium is required for mTORC1 activation (36–38). First, we checked mTORC1 activity by Western blot analysis upon IP3R3 depletion. As shown by mTORC1-mediated S6 kinase 1 (S6K1) Thr389 phosphorylation and subsequent S6 Ser240/244 phosphorylation, mTORC1 activity was abolished when IP3R3 was depleted in MDA-MB-468 cells (Fig. 4H). We also observed modest, but consistent, mTORC1 activity downregulation by knocking down BBOX1 in MDA-MB-468 and HCC70 cells (Fig. 4I; Supplementary Fig. S6C). To further validate that calcium is required for mTORC1 activation in TNBC, we treated BBOX1 KD cells with the ER Ca^{2+}-ATPase inhibitor thapsigargin (Tg), which causes a rapid

Figure 3. BBOX1 interacts with IP3R3 and regulates its stability. **A,** Schematic strategy of TAP-TAG purification by mass spectrometry. **B,** Lists of BBOX1-binding proteins identified by mass spectrometry (MS). IP3R3 is a BBOX1 interactor identified by two rounds of immunoprecipitation followed by MS. **C,** Coimmunoprecipitation (co-IP) of endogenous IP3R3 and exogenous HA-tagged wild-type BBOX1 or N2D mutant in MDA-MB-231 stable cell lines. **D,** Co-IP of endogenous BBOX1 and IP3R3 in HCC70 cells. **E,** Immunoblot analysis of IP3 receptor family protein (IP3R1, 2, and 3) level in indicated BBOX1-depleted TNBC cell lines. N.D., not detected. **F,** Immunoblot analysis of IP3R3 and BBOX1 protein level in doxycycline-inducible BBOX1 knockdown MDA-MB-468 cells. **G,** Immunoblot analysis of MDA-MB-468 lines infected with lentivirus encoding shRNA control or *BBOX1* sh1 followed by treatment with neddylation inhibitor MLN-4924 or proteasomal inhibitor MG132. HIF1α was used as a control for the efficacy of the inhibitor treatment. Numbers indicate quantification of the IP3R3 blot. **H,** Ubiquitin assay followed by immunoblotting of MDA-MB-468 and HCC70 cells infected with control or *BBOX1* shRNAs. **I,** MDA-MB-468 cells infected with lentivirus encoding control or *BBOX1* shRNAs were treated with cycloheximide (CHX) for the indicated times. Cells were subsequently harvested for immunoblotting as indicated. The graph below shows the quantification of IP3R3 levels from two independent experiments. **J,** Immunoblot of lysates from MDA-MB-468 stable cells expressing FBXL2, or treated with MG132. Numbers indicated quantification of the IP3R3 blot. **K,** 293T cells were cotransfected with V5-tagged FBXL2, FLAG-IP3R3 truncated mutant (227–602), and increasing amounts of HA-tagged BBOX1 or N2D for 48 hours. Cells were harvested for IP with anti-FLAG beads and proteins were immunoblotted as indicated. This experiment was conducted twice. **L,** 293T cells were cotransfected with V5-tagged FBXL2, increasing amounts of FLAG-tagged BBOX1 as indicated for 36 hours, then cells were treated with MG132 overnight before ubiquitin assay. This experiment was conducted twice. **M,** Immunoblot analysis of IP3R3 and BBOX1 protein level in MDA-MB-468–stable cell lines expressing control vector (Vector), wild-type BBOX1 (BBOX1), or N2D mutant (N2D) followed by infection of indicated shRNA lentivirus. * indicates exogenous BBOX1 proteins. Numbers indicate quantification of the IP3R3 blot. **N,** Immunoblot of endogenous IP3R3 and BBOX1 protein levels in a panel of normal breast epithelial cell lines and breast cancer cell lines. **O** and **P,** Representative IHC staining images (**O**) and quantification (**P**) of human breast tumor specimens with four staining grades showing the expression correlation between BBOX1 and IP3R3 protein. H Score was used for indicating the immunostaining intensity of the sample. According to the distribution of the H Scores, 1–60 was assigned as grade I, 61–120 as grade II, 121–180 as grade III, and 181–300 as grade IV. WCL, whole cell lysates.

Published OnlineFirst July 20, 2020; DOI: 10.1158/2159-8290.CD-20-0288

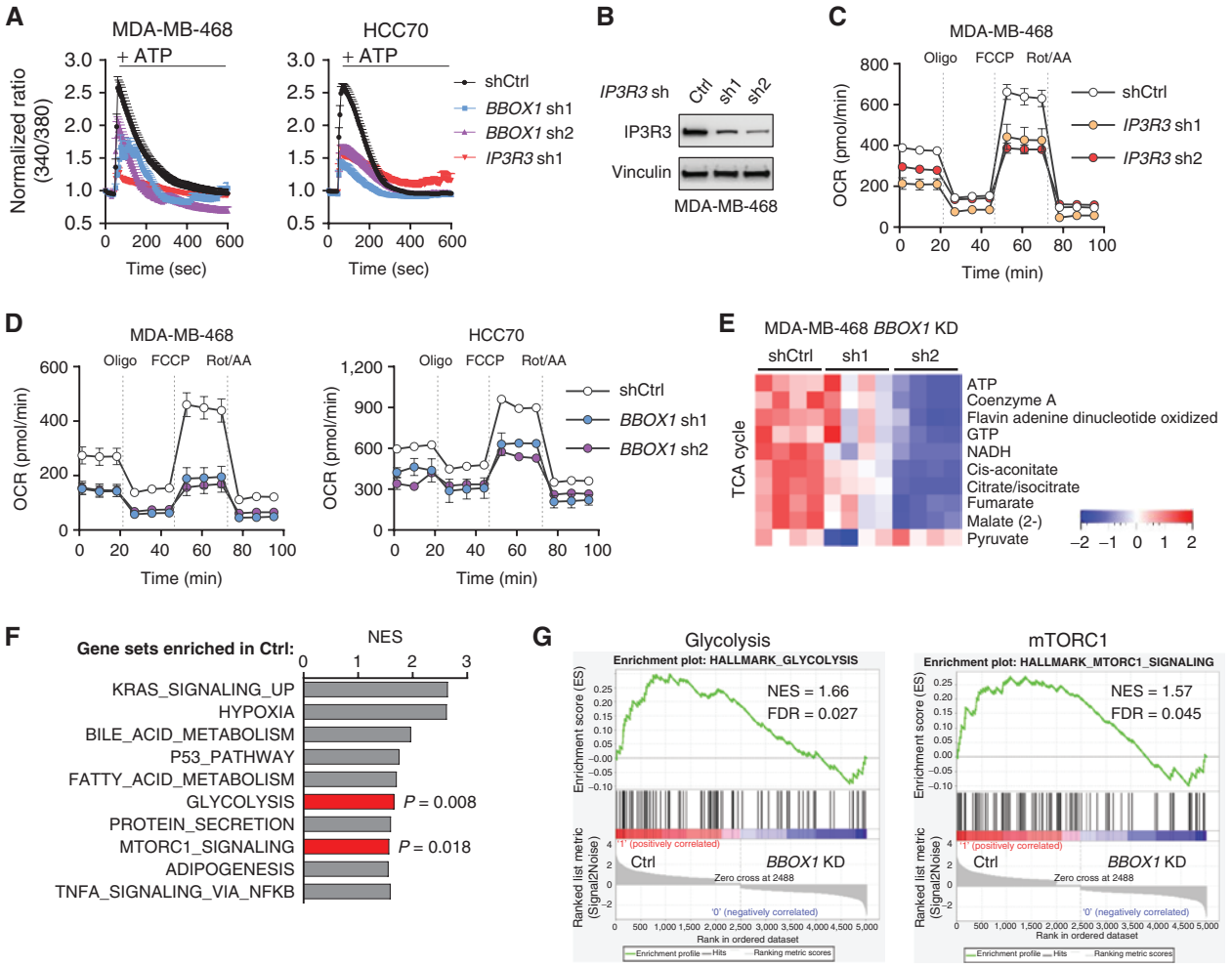

Figure 4. BBOX1 sustains IP3R3-mediated calcium signaling that is required for mitochondrial activity and mTORC1-dependent glycolysis. **A,** Measurement of ER calcium release upon ATP stimulation in indicated cells infected with control, *BBOX1* or *IP3R3* shRNAs. **B** and **C,** Immunoblot (**B**) and measurement of OCR (**C**) in control or IP3R3-depleted MDA-MB-468 cells. **D,** Measurement of OCR in control or BBOX1-depleted MDA-MB-468 and HCC70 cells. **E,** Heat map of the TCA cycle–related metabolites in control or BBOX1-depleted MDA-MB-468 cells in the metabolomics analysis. **F,** Normalized Enrichment Score (NES) plot of the "hallmark" signatures gene sets enriched in the control MDA-MB-468 cells. **G,** GSEA of the differentially expressed genes for glycolysis and mTORC1 pathways. (*continued on following page*)

increase of cytosolic calcium (39), or cotreated them with Tg and the calcium chelator ethylene glycol tetra-acetic acid (EGTA) to remove extracellular calcium. We found that Tg treatment rescued the decreased mTORC1 activity in BBOX1 KD cells, and this effect was ameliorated by cotreatment with EGTA (Supplementary Fig. S6D). These data demonstrated that mTORC1 signaling could be activated by BBOX1–IP3R3-mediated calcium signaling. We next measured the extracellular acidification rate (ECAR) as an indicator of glycolysis in IP3R3- or BBOX1-depleted cells, and found that the glycolytic rate was decreased upon both IP3R3 and BBOX1 depletion (Fig. 4J and K; Supplementary Fig. S6E). Collectively, our data show that BBOX1 is also required for maintaining glycolysis through IP3R3-mediated calcium signaling in TNBC cells.

The mitochondrial respiration, mTORC1 activity, and glycolysis deficiency induced by BBOX1 depletion subsequently corresponded with increased apoptosis measured by upregulated cleaved PARP, which was confirmed by flow cytometry analysis (Fig. 4L; Supplementary Fig. S7A–S7D). On the contrary, overexpression of BBOX1, but not the N2D mutant, protected TNBC cells from apoptosis as shown by cleaved PARP for the basal apoptotic level (Supplementary Fig. S7E). IP3R3 depletion in these TNBC cell lines recapitulated the apoptotic phenotype observed with BBOX1 knockdown (Fig. 4M; Supplementary Fig. S7F–S7H). Furthermore, we found that the G_2–M cell-cycle checkpoint was strongly enriched in BBOX1 KD cells (Supplementary Fig. S8A and S8B), which was further confirmed by cell-cycle analysis by flow cytometry with BBOX1 or IP3R3 depletion (Supplementary Fig. S8C–S8F). To validate IP3R3 as a critical downstream target of BBOX1 for TNBC cell growth, we depleted IP3R3 in multiple TNBC cell lines and found decreased cell proliferation with MTS assay, 2-D colony formation assay, and 3-D soft-agar formation (Fig. 4N; Supplementary Fig. S9A–S9D). Notably, IP3R3 depletion in MCF-10A and HMLE cells did not cause a significant cell growth defect (Fig. 4N; Supplementary Fig. S9E and

Published OnlineFirst July 20, 2020; DOI: 10.1158/2159-8290.CD-20-0288

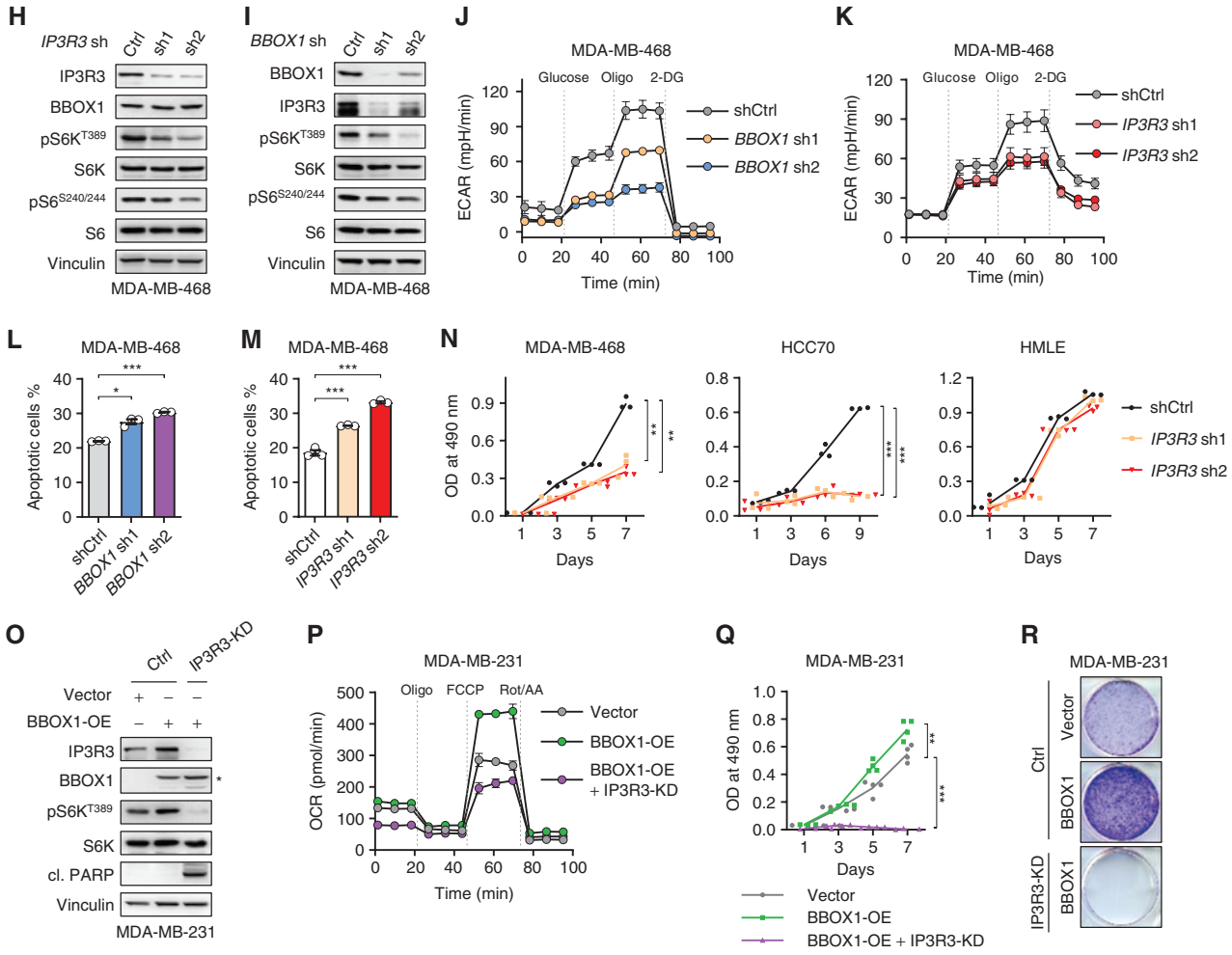

Figure 4. ***(Continued)*** **H** and **I,** Immunoblot of lysates from BBOX1 (**H**) or IP3R3 (**I**) depleted MDA-MB-468 cell lines. **J** and **K,** Measurement of ECAR in BBOX1 (**J**) or IP3R3 (**K**) depleted MDA-MB-468 cells. **L** and **M,** Quantification of the apoptotic cells in indicated BBOX1 (**L**) or IP3R3 (**M**) depleted MDA-MB-468 cells analyzed by flow cytometry. **N,** MTS cell proliferation assay of indicated TNBC cells or normal breast epithelial HMLE cells infected with lentivirus encoding control or *IP3R3* shRNAs. **O–R,** Immunoblot (**O**), OCR (**P**), MTS proliferation (**Q**), and colony formation (**R**) of MDA-MB-231–stable cell lines expressing control vector (Vector), wild-type BBOX1 (BBOX1-OE) followed by infection of indicated control (Ctrl) or *ITPR3* shRNA (IP3R3-KD). * in **O** indicates exogenous BBOX1 proteins. Error bars, SEM, two-tailed Student *t* test (*, $P < 0.05$; **, $P < 0.01$; ***, $P < 0.001$).

S9F). To examine whether the phenotypic effects of BBOX1 on TNBC or breast epithelial cells are dependent on IP3R3, we overexpressed BBOX1 in multiple cell lines and observed increased S6K1 Thr389 phosphorylation, OCR, and cell proliferation, effects that were ameliorated by concurrent IP3R3 depletion (Fig. 4O–R; Supplementary Fig. S9G–S9L). It is worth noting that IP3R3 did not associate with poor prognosis in TNBC/basal cancers (Supplementary Fig. S9M), which could be due to its posttranscriptional regulation by BBOX1. Collectively, our results suggest that IP3R3 is an important downstream functional mediator of the effects of BBOX1 on TNBC cell proliferation and survival. In addition, the effect of BBOX1 on cell proliferation could be multifactorial, by affecting mTORC1/glycolysis as well as mitochondrial function.

BBOX1 Is a Therapeutic Target in TNBC

To examine the physiologic relevance of targeting the BBOX1 signaling pathway in TNBC *in vivo*, we first generated cell lines with BBOX1 knockdown by using two independent shRNAs. We orthotopically injected these cells into the mammary fat pad of immunocompromised NOD/SCID gamma (NSG) mice and monitored the tumor growth over time. Consistent with the phenotype observed *in vitro*, BBOX1 depletion led to a profound breast tumor growth defect *in vivo*, which correlated with decreased IP3R3 in tumors (Fig. 5A–C; Supplementary Fig. S10A). In addition, we also generated doxycycline-inducible BBOX1 knockdown MDA-MB-468 cells with two independent shRNAs. In these cells, BBOX1 can be efficiently depleted upon doxycycline treatment, which led to efficient inhibition of 2-D colony formation as well as 3-D anchorage-independent growth (Fig. 5D–G). Then, one of these hairpin-infected tumor cells and the control cells were orthotopically injected into the mammary fat pad of NSG mice. Upon confirmation of tumor formation, we fed these mice doxycycline to induce BBOX1 depletion. Whereas control cells (shCtrl) grew readily over time, BBOX1 depletion

Published OnlineFirst July 20, 2020; DOI: 10.1158/2159-8290.CD-20-0288

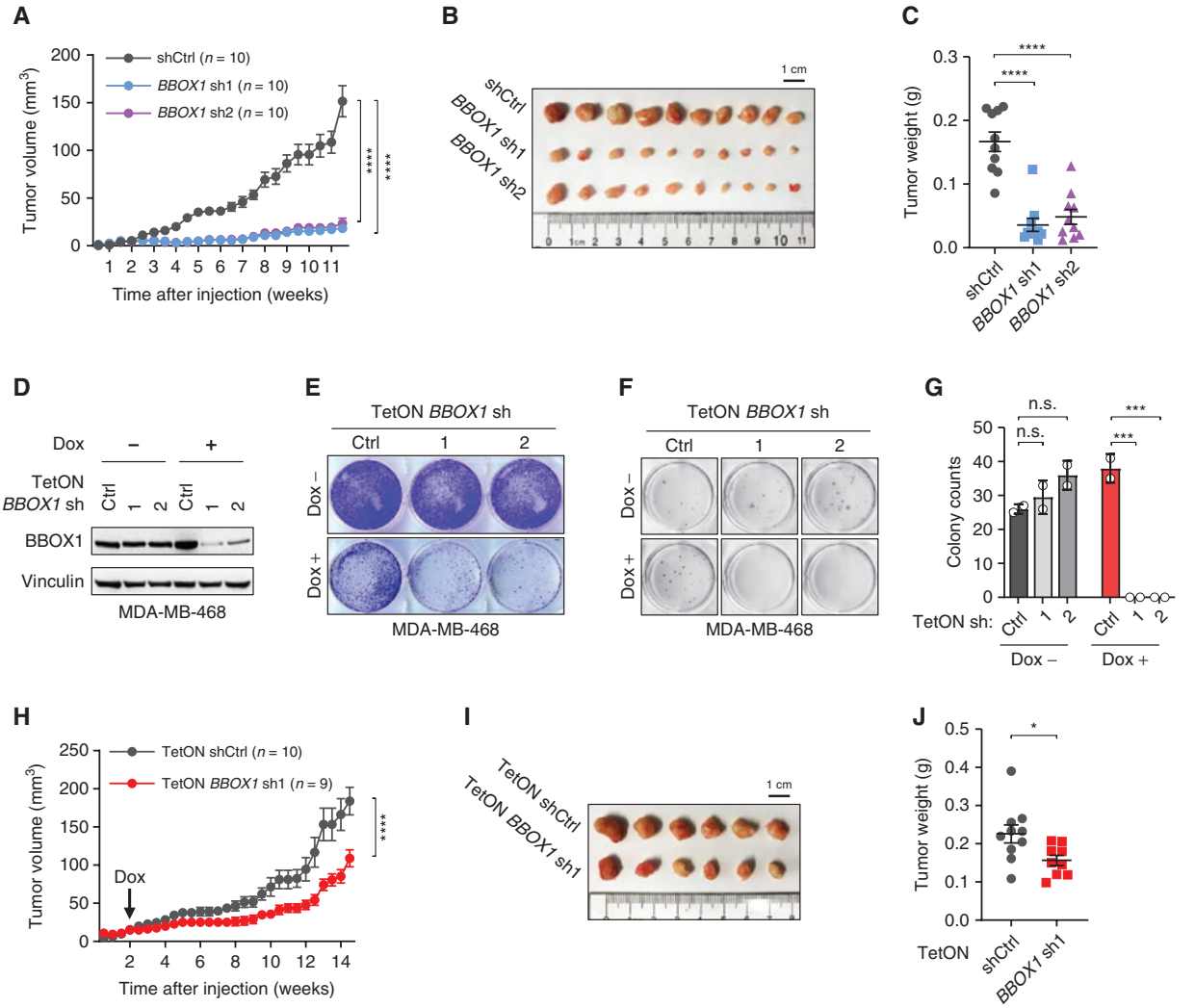

Figure 5. Depletion of BBOX1 suppresses TNBC tumorigenesis. **A–C,** Tumor growth (**A**), image of tumors (**B**), and tumor weight after dissection (**C**) of MDA-MB-468 cells infected with lentivirus encoding control or *BBOX1* shRNAs injected orthotopically at the mammary fat pad of NSG mice. $n = 10$. **D–G,** Immunoblot analysis (**D**), 2-D colony formation (**E**), 3-D soft-agar growth (**F**), and soft-agar colony quantification (**G**) of inducible BBOX1 KD MDA-MB-468 cells treated with or without doxycycline. **H–J,** Tumor growth (**H**), image of tumors (**I**), and tumor weight after dissection (**J**) of doxycycline-inducible BBOX1 KD MDA-MB-468 cells injected orthotopically at the mammary fat pad of NSG mice. Treatment of doxycycline food started at indicated time. Statistical analysis was conducted by one-way ANOVA followed by Tukey multiple comparison test (**A** and **H**) or two-tailed Student *t* test (**C**, **G**, and **J**). Error bars, SEM (*, $P < 0.05$; **, $P < 0.01$; ***, $P < 0.001$; ****, $P < 0.0001$; n.s., no significance).

significantly inhibited tumor growth and downstream IP3R3 levels (Fig. 5H–J; Supplementary Fig. S10B). These data suggest that BBOX1 is important for maintaining TNBC tumor growth *in vivo*. It is important to note that tumor phenotype was more robust in Fig. 5A compared with Fig. 5H, which may be due to a longer time for doxycycline-inducible shRNAs to take effect *in vivo* compared with noninducible shRNAs.

As an orthogonal approach, we next investigated the pharmacologic inhibition of BBOX1. To this end, we implemented Mildronate (40), a clinically approved drug in a limited setting, and two leading recently characterized BBOX1 inhibitor compounds: C-2124 (41) and AR692B (42). Mildronate and C-2124 are structural analogues of the BBOX1 enzymatic substrate GBB that abolish BBOX1 catalytic activity through competitive binding to its substrate pocket. AR692B, on the other hand, causes BBOX1 conformational changes (42). First, we tested the effect of these inhibitors on disrupting the BBOX1–IP3R3 interaction. In fact, all these compounds inhibited the association between BBOX1 and IP3R3 endogenously or exogenously in multiple cell lines including MDA-MB-468 and MDA-MB-231 in a dose-dependent manner (Fig. 6A–D; Supplementary Fig. S11A–S11G), which is consistent with the data we obtained with the BBOX1 catalytically dead mutant N2D. Next, we treated MDA-MB-468 cells with C-2124, Mildronate, or AR692B and found that these treatments led to decreased IP3R3 protein levels after extended-period treatment (72 or 96 hours), whereas no effect was observed after short-term treatment (24 hours; Supplementary Fig. S11H–S11J). In addition, mTORC1 signaling was significantly suppressed by these inhibitor treatments (Fig. 6E and F;

Published OnlineFirst July 20, 2020; DOI: 10.1158/2159-8290.CD-20-0288

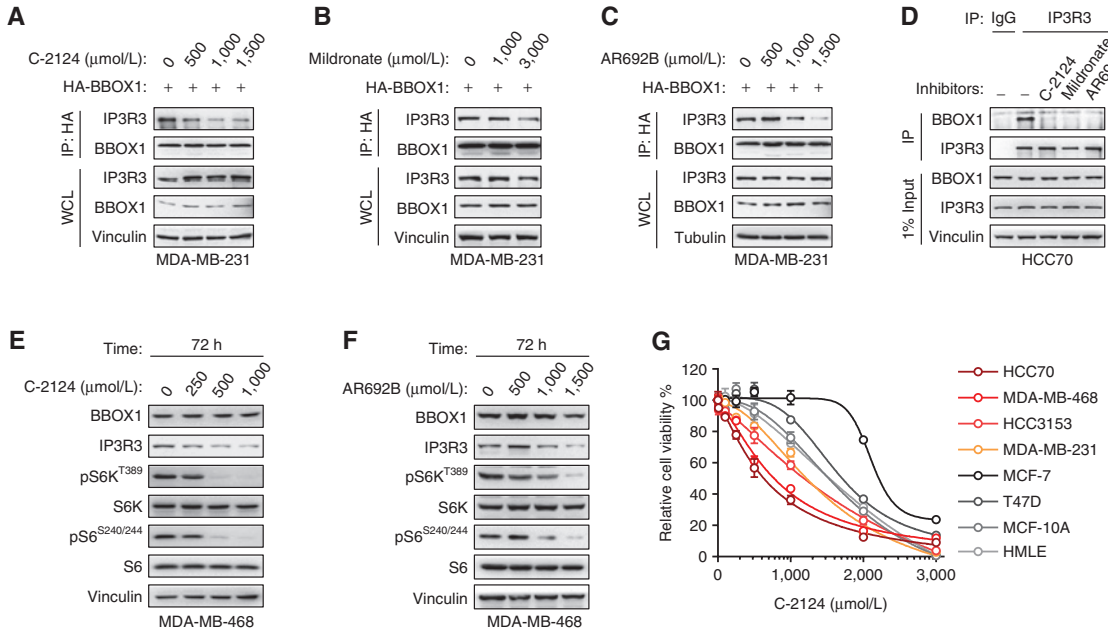

Figure 6. BBOX1 is a therapeutic target for TNBC. **A–C,** Co-IP of HA-tagged BBOX1 and endogenous IP3R3 in MDA-MB-231 cells treated with the indicated amount of C-2124 (**A**), Mildronate (**B**), and AR692B (**C**) overnight. WCL, whole cell lysates. **D,** Co-IP of endogenous BBOX1 and IP3R3 in HCC70 cells treated with indicated BBOX1 inhibitors for overnight. The dosage of inhibitors used is 1.5 mmol/L for C-2124 and AR692B, and 5 mmol/L for Mildronate. **E** and **F,** Immunoblot analysis of MDA-MB-468 cells treated with an indicated dosage of C-2124 (**E**) or AR692B (**F**) for 72 hours. **G,** Cell viability assay of breast cancer cells or normal breast epithelial cells treated with increasing doses of C-2124. Results for each cell line are normalized to untreated cells. (*continued on next page*)

Supplementary Fig. S11K and S11L). In line with the OCR decrease induced by BBOX1 depletion, C-2124 treatment also led to impaired OCR in MDA-MB-468 cells (Supplementary Fig. S11M). Cell viability was then assessed by treating a panel of breast cancer cell lines with various doses of the inhibitors C-2124 or AR692B. We observed that the TNBC cell lines with high BBOX1 expression (e.g., MDA-MB-468, HCC70) displayed higher sensitivity to the BBOX1 inhibitors compared with the non-TNBC cell lines with low BBOX1 expression (e.g., MCF-7, T47D, MCF-10A; Fig. 6G; Supplementary Fig. S12A). Notably, this sensitivity was especially obvious in the range of low doses for these inhibitors. Furthermore, we conducted 3-D soft-agar assays in these cells and found that these inhibitors suppressed anchorage-independent growth in TNBC cell lines including MDA-MB-468, HCC70, HCC3153, or MDA-MB-231 in a dose-dependent manner. Interestingly, these inhibitors did not affect MCF-7, T47D, or HMLE cell growth (Fig. 6H; Supplementary Fig. S12B–S12D), despite the fact that the intercellular carnitine level was profoundly decreased by BBOX1 inhibitor treatment in these cells (Supplementary Fig. S12E). Therefore, BBOX1 protein level correlates to some extent with the efficacy of BBOX1 inhibitors in these cells. In addition, 2-D colony formation assay showed that these inhibitors did not affect MCF-10A cell growth (Supplementary Fig. S12F and S12G). To further assess the specificity of the inhibitor, we treated MDA-MB-231 cells stably expressing WT BBOX1 or N2D mutant with various doses of C-2124 or vehicle. The cell viability assay showed that MDA-MB-231 cells expressing WT BBOX1 exhibited higher sensitivity compared with MDA-MB-231 N2D cells (Fig. 6I). As a proof of principle, we examined the efficacy of the BBOX1 inhibitor *in vivo*. We treated MDA-MD-468 xenograft breast tumor–bearing NSG mice with Mildronate and found that it efficiently suppressed tumor growth *in vivo* (Fig. 6J–L). Importantly, these treatments did not affect body weight (Fig. 6M), suggesting that the drug does not carry significant toxicity in mice and the effect of these BBOX1 inhibitors on TNBC is specific.

DISCUSSION

In this study, we have identified BBOX1 as a potential new target in TNBC by modulating IP3R3 protein stability, calcium homeostasis, cellular bioenergetics, and cancer cell fate. In summary, BBOX1 protects IP3R3 from FBXL2-mediated proteasomal degradation and maintains IP3R3-mediated constitutive calcium flux from ER that is essential for sustaining mitochondrial function and activating mTORC1-mediated glycolysis. Both metabolic pathways are critical for meeting the demand of energy and biochemical intermediates for cancer cell proliferation and tumorigenesis. On the other hand, either *BBOX1* genetic depletion or pharmacologic abrogation of the BBOX1–IP3R3 interaction blocks this oncogenic calcium signaling, impairing cellular metabolism and eventually causing cancer cell death (Fig. 6N).

TNBC is a heterogeneous and lethal disease among women, with limited therapeutic options (43), and discovery of new targeted therapies is required. We performed the initial screening from a library targeting the whole family of known 2-OG–dependent enzymes because: (i) they play a role as oxygen sensors in the mammalian cell to regulate a broad spectrum of cellular processes; for instance, the proline hydroxylase EGLNs governs HIFα protein stability regulation under

Published OnlineFirst July 20, 2020; DOI: 10.1158/2159-8290.CD-20-0288

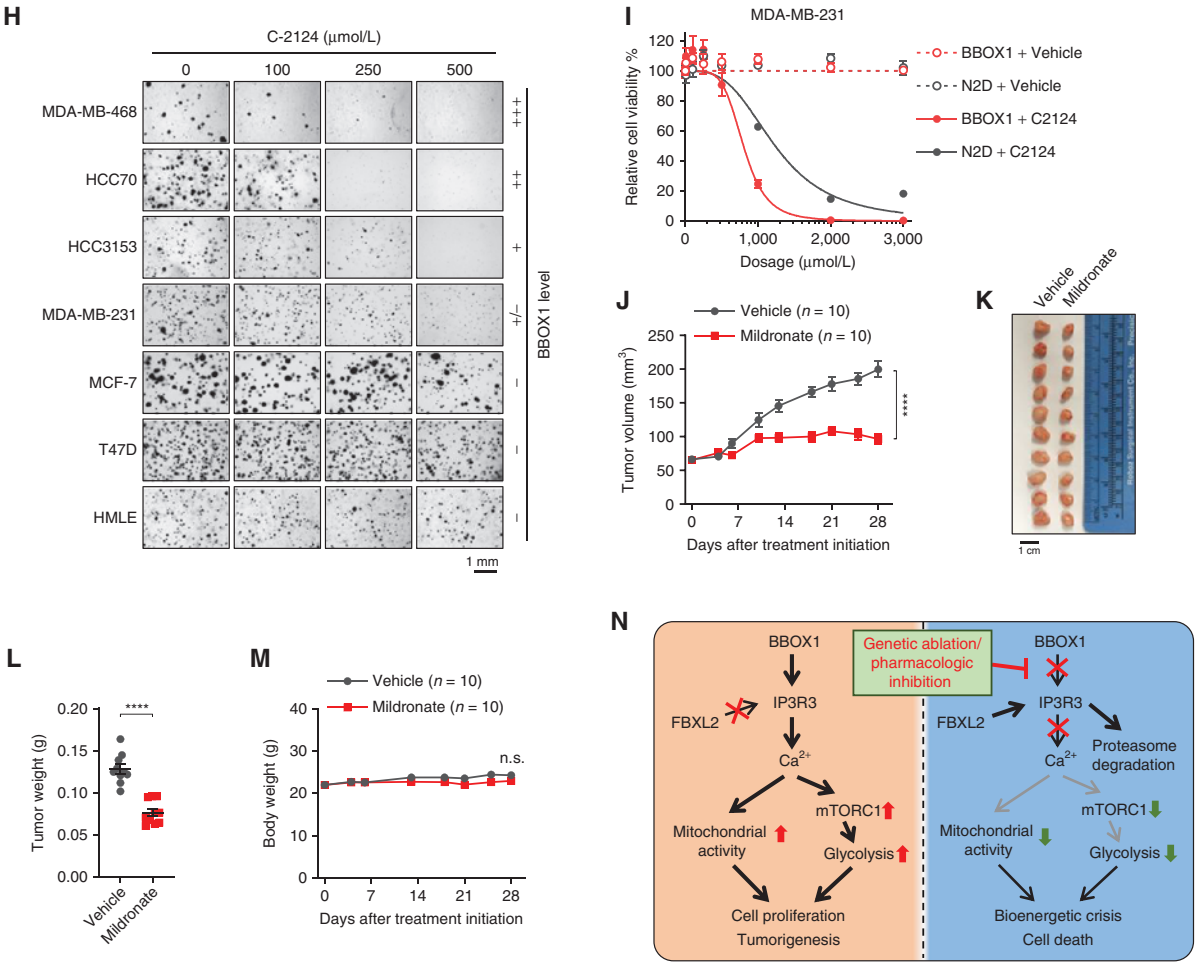

Figure 6. ***(Continued)*** **H,** Soft-agar colony growth of indicated cell lines treated with the indicated amount of C-2124. BBOX1 expression level of cells was indicated according to Fig. 1F. **I,** Dose–response curves for MDA-MB-231 cells overexpressing either wild-type BBOX1 or catalytic mutant N2D. **J–M,** Tumor growth (**J**), image of tumors (**K**), tumor weight after dissection (**L**), and body weight (**M**) of MDA-MB-468 xenograft NSG mice treated with Mildronate. **N,** Schematic model of the mechanism proposed for this study. Statistical analysis was conducted by one-way ANOVA followed by Tukey multiple comparison test (**J** and **M**) or two-tailed Student *t* test (**L**). Error bars, SEM (*, $P < 0.05$; **, $P < 0.01$; ***, $P < 0.001$; ****, $P < 0.0001$; n.s., no significance).

different oxygen scenarios (normoxia/hypoxia), therefore contributing to malignancies in cancer (44); (ii) emerging literature has uncovered their critical roles in cancer progression or suppression, while an unbiased systematic approach to investigate their role in cancer is lacking; (iii) there are actionable therapeutic drugs that have been or can be developed to target some of these enzymes (45). In this article, we show a previously unrecognized role of BBOX1 in breast cancer tumorigenesis, independent of its canonical function in carnitine synthesis. By TAP-TAG purification followed by mass spectrometry, we identify IP3R3 as an important binding partner and downstream factor of BBOX1. Our finding indicates the role of the 2-OG–dependent enzymes in regulating numerous noncanonical substrates or binding partners, which deserves further investigation. One limitation of our study is that we have not demonstrated whether BBOX1 can catalyze hydroxylation reactions beyond GBB and use large molecules such as proteins as substrates. We speculate that this is highly possible because IP3R3 binding with BBOX1 largely depends on its catalytic activity, which warrants further investigation.

Calcium signaling plays vital roles in various cellular processes (46) and has been largely reported to associate with cancer progression (47, 48). Calcium-dependent signaling pathways are frequently dysregulated or altered in cancer cells to meet the demand of cell proliferation, invasion, and metastasis (47). The IP3 receptors are principal Ca^{2+} channels located on the ER membrane and essential for the control of intracellular Ca^{2+} levels (49). There are three IP3R family members (IP3R1, IP3R2, and IP3R3), and IP3R3 is emerging as the isoform that is particularly important in the pathogenesis of human diseases (50). Increases of IP3R3 expression occur in a variety of malignancies, such as colorectal cancer, glioblastoma, breast cancer, and kidney cancer (23–26). Previous studies reported that IP3R3-mediated calcium signaling positively regulates migration (31) and cell growth under certain conditions (51) in the MCF-7 breast cancer cell line. Our study confirms the universal role of calcium and highlights that TNBC cells are particularly addicted to the IP3R3–Ca^{2+} signaling axis. We identify BBOX1 as an upstream regulator of this IP3R3–Ca^{2+} signaling controlling various critical metabolic pathways (e.g.,

Published OnlineFirst July 20, 2020; DOI: 10.1158/2159-8290.CD-20-0288

TCA cycle, glycolysis, and nucleotide metabolism). BBOX1 depletion–induced cell-cycle changes may be largely due to its effect on calcium signaling, because it is well documented that calcium is a critical regulator of cell-cycle progression (47). Therefore, targeting aberrant calcium signaling may be beneficial for certain cancers such as TNBC (52).

In this study, we incorporated several BBOX1 inhibitors to target TNBC cell growth and tumorigenesis *in vitro* and *in vivo*. As a proof-of-principle of our finding, these inhibitors showed some efficacy by blocking the BBOX1–IP3R3 interaction, suppressing oncogenic calcium signaling, altering cell metabolism, and killing TNBC cells. Meldonium (trade name Mildronate), developed in 1970 by the Latvian Institute of Organic Synthesis, is widely used as an antiischemia drug in eastern Europe, and was shown to be safe and well tolerated (53, 54). According to previous literature, the K_m of meldonium toward rat BBOX1 was 37 μmol/L (55), which explains why we need a relatively high dosage to be used in human cancer cell lines. However, it is important to point out that at the dosage used, these inhibitors did not appear to affect normal breast epithelial cell proliferation (Fig. 6H; Supplementary Fig. S12C and S12D). These inhibitors appear to be nontoxic in multiple models used, including dogs and rats (56). For example, 800 mg/kg was used in the rat model with no obvious toxicity (57). However, it is important to acknowledge that meldonium might likely inhibit OCTN2 (58). In addition, we have not examined the drug in more clinically relevant models such as patient-derived xenografts. Novel BBOX inhibitors have been developed and show better selectivity and efficacy to some extent (41, 42), as we also observed in our study. In summary, our study provides evidence that BBOX1 is a new therapeutic target in TNBC, which hopefully will motivate the development of specific and potent BBOX1 inhibitors in this lethal disease.

METHODS

Cell Culture

MDA-MB-231, MDA-MB-436, Hs578T, MCF-7, BT474, and 293T cells were cultured in DMEM (Gibco 11965118) supplemented with 10% FBS and 1% penicillin–streptomycin. T47D, HCC3153, HCC1187, HCC70, and MDA-MB-468 cells were cultured in 10% FBS, 1% penicillin–streptomycin RPMI 1640 (Gibco, 11875093). Normal breast epithelial cells HMLE and MCF-10A were cultured in Mammary Epithelial Growth Medium (Lonza CC-3151) containing SingleQuots Supplements (Lonza CC-4136). SUM149 cells were cultured in HuMEC Ready Medium (Gibco, 12752-010). HCC3153 cells were obtained from the cell repository of the Hamon Center for Therapeutic Oncology Research, UT Southwestern Medical Center (Dallas, TX). HMLE cells were obtained from Dr. Wenjun Guo, Albert Einstein College of Medicine. All other cell lines were obtained from ATCC. Cells were used for experiments within 10 to 20 passages from thawing. All cells were authenticated via short tandem repeat testing. *Mycoplasma* detection was routinely performed using the MycoAlert Detection Kit (Lonza, LT07-218).

Antibodies and Reagents

Rabbit anti-BBOX1 (ab171959) and goat anti-FBXL2 (ab17018) were from Abcam. Mouse anti-IP3R3 (610312) was from BD Biosciences. Rabbit anti-TMLHE (16621-1-AP) and rabbit anti-ALKBH4 (19882-1-AP) were from ProteinTech. Rabbit anti-HIF1α (3716), rabbit anti-PTEN (9559S), rabbit anti-HA tag (3724), rabbit anti-FLAG-tag (14793), rabbit anti-V5-tag (13202), mouse anti-His-tag (2366), rabbit anti-cleaved-caspase 3 (9664), rabbit anti-PARP (9532), and mouse anti-α-Tubulin (3873) were from Cell Signaling Technology. Mouse anti-Ub (8017) and mouse anti-β-actin (sc-47778) were from Santa Cruz Biotechnology. Mouse anti-vinculin (V9131) was from Sigma-Aldrich. Antibodies used for IHC staining were rabbit anti-IP3R3 (Bethyl Laboratories, 50-157-2451) and mouse anti-BBOX1 (Sigma-Aldrich, WH0008424M1). Mildronate (S4130) was from Selleckchem. C-2124 was kindly provided by the Latvian Institute of Organic Synthesis (41). AR692B was synthesized by WuxiAPP Tech following the procedure described previously (42). MTS reagents (ab197010) were from Abcam. Doxycycline (D9891) and MLN-4924 (5054770001) were from Sigma-Aldrich, DMOG (D1070-1g) was from Frontier Scientific, and MG132 (IZL-3175-v) was from Peptide International.

2-D Cell Proliferation Assay and 3-D Soft-Agar Growth Assay

For MTS assay, cells were seeded in 96-well plates (1,000–2,000 cells/well) in appropriate growth medium; the rest of the steps were performed as described previously (59). The colony formation assay and 3-D soft-agar assay were performed as described previously (60). For colony formation assay, cells were seeded in duplicate in 6-well plates (1×10^5 cells/well). For inhibitor treatments, BBOX1 inhibitors were added the following day after seeding the cells and were renewed every day.

Immunoblotting and Immunoprecipitation

EBC buffer (50 mmol/L Tris-HCl pH 8.0, 120 mmol/L NaCl, 0.5% NP40, 0.1 mmol/L EDTA, and 10% glycerol) supplemented with complete protease inhibitor and phosphoSTOP tablets (Roche Applied Bioscience) was used to harvest whole-cell lysates at 4°C. Cell lysate concentration was measured by Protein Assay Dye (Bio-Rad). Equal amount of cell lysates was resolved by SDS-PAGE. For immunoprecipitation, whole-cell lysates were prepared in EBC buffer supplemented with protease inhibitor and phosphatase inhibitor. The lysates were clarified by centrifugation and then incubated with primary antibodies or FLAG/HA antibody–conjugated beads (FLAG M2 beads, Sigma; HA beads, Roche Applied Bioscience) overnight at 4°C. For primary antibody incubation, cell lysates were incubated further with protein G sepharose beads (Roche Applied Bioscience) for 2 hours at 4°C. The bound complexes were washed with EBC buffer 3 times and were eluted by boiling in SDS loading buffer. Bound proteins were resolved in SDS-PAGE followed by immunoblotting analysis.

RNA-seq Analysis

Total RNA from triplicates was extracted from MDA-MB-468 cells infected with control or BBOX1 shRNAs by using RNeasy kit with on column DNase digestion (Qiagen). Library preparation and sequencing were performed by BGI as paired-end 100-bp reads followed by the same analysis pipeline as described previously (59). GSEA was performed by using the GSEA software and Hallmark signatures. RNA-seq data are deposited to GEO under accession number GSE152317.

OCR and ECAR Measurement

The OCR and ECAR were measured by an XFe24 extracellular flux analyzer (Agilent Technologies), according to the manufacturer's instructions. Briefly, a total of 1×10^5 cells were seeded into XF24 cell culture microplate coated with CellTak (Corning) before the assay. Detailed experimental procedures are described in the Supplementary Methods.

Survival Analysis

The effects of *BBOX1* gene and IP3 receptor family genes (*ITPR1, 2*, and *3*) on the survival of patients with breast cancer were performed using the Kaplan–Meier Plotter online survival analysis tool (https://kmplot.com/analysis/). To obtain sufficient patient

Published OnlineFirst July 20, 2020; DOI: 10.1158/2159-8290.CD-20-0288

samples, the relapse-free survival mode was used to conduct all the analyses.

Orthotopic Tumor Xenograft

Six-week-old female NSG mice (Jackson Laboratory) were used for xenograft studies. Approximately 5×10^5 viable MDA-MB-468 cells expressing control/BBOX1 shRNAs or TetON BBOX1 shRNA, or 1×10^6 viable MDA-MB-468 parental cells, were resuspended in 100 μL Matrigel (Corning, 354234) and injected orthotopically into the mammary fat pad of each mouse. For inducible BBOX1 shRNA, after cell injection and following two consecutive weeks of tumor monitoring to make sure tumor was successfully implanted, mice were fed Purina rodent chow with doxycycline (Research Diets Inc., #5001). For BBOX1 inhibitor treatment, when tumors reached the volume of approximately 60 mm^3, mice were divided in two groups by randomization, and 400 mg/kg body weight of Mildronate or the vehicle saline was given through intraperitoneal injection. Tumor size was measured using an electronic caliper. Tumor volumes were calculated with the formula: volume = $(L \times W^2)/2$, where L is the tumor length and W is the tumor width measured in millimeters. All animal experiments were in compliance with NIH guidelines and were approved by the University of North Carolina at Chapel Hill and The University of Texas Southwestern Medical Center Animal Care and Use Committee.

Statistical Analysis

All statistical analysis was conducted using Prism 8.0 (GraphPad Software). All graphs depict mean ± SEM unless otherwise indicated. Statistical significances are denoted as n.s. (not significant; $P > 0.05$); *, $P < 0.05$; **, $P < 0.01$; ***, $P < 0.001$; ****, $P < 0.0001$. The numbers of experiments are noted in figure legends. To assess the statistical significance of a difference between two conditions, we used unpaired two-tailed Student t test. For experiments comparing more than two conditions, differences were tested by a one-way ANOVA followed by Dunnett or Tukey multiple comparison tests.

Disclosure of Potential Conflicts of Interest

J.W. Locasale reports personal fees from Restoration Foodworks, other from Raphael Pharmaceuticals, and personal fees from Nanocare Technologies outside the submitted work. C.M. Perou reports personal fees from Bioclassifier LLC (C.M. Perou is an equity stock holder and consultant of BioClassifier LLC) outside the submitted work; in addition, C.M. Perou has a patent for U.S. Patent no. 12,995,459 licensed and with royalties paid from Veractye (patent pertains to gene expression subtyping assay). No potential conflicts of interest were disclosed by the other authors..

Authors' Contributions

C. Liao: Conceptualization, data curation, software, formal analysis, supervision, validation, investigation, visualization, methodology, writing-original draft, project administration, writing-review and editing. **Y. Zhang:** Formal analysis, methodology, performed the calcium measurement. **C. Fan:** Software, formal analysis, methodology, performed the patient data analysis. **L.E. Herring:** Software, formal analysis, methodology. **J. Liu:** Software, methodology. **J.W. Locasale:** Methodology, performed the metabolomics study. **M. Takada:** Validation. **J. Zhou:** Validation, acquisition of data during revision. **G. Zurlo:** Writing-review and editing. **L. Hu:** Validation. **J.M. Simon:** Software, formal analysis. **T.S. Ptacek:** Software, formal analysis. **V.G. Andrianov:** Resources, inhibitors synthesis. **E. Loza:** Resources. **Y. Peng:** Validation, methodology. **H. Yang:** Methodology. **C.M. Perou:** Supervision, funding acquisition. **Q. Zhang:** Conceptualization, data curation, supervision, funding acquisition, validation, investigation, methodology, writing-original draft, project administration, writing-review and editing.

Acknowledgments

This work was supported by the Cancer Prevention and Research Institute of Texas (to Q. Zhang, CPRIT, RR190058), American Cancer Society (to Q. Zhang, RSG-18-059-01-TBE), NCI Breast SPORE program (to C.M. Perou, P50-CA58223), NCI (to C.M. Perou, R01-CA148761), and BCRF (to C.M. Perou). We thank all members of the Zhang, Perou, and Yang laboratories for helpful discussions and suggestions. We thank Dr. Ralph DeBerardinis and Children's Research Institute's Metabolomics Facility at UTSW for their help. We thank Dr. Shafi Kuchay and Dr. Michele Pagano for providing the IP3R3-mutant plasmids. We thank Dr. Osvalds Pugovics for help with BBOX1 inhibitors. We thank Yongjuan Xia, Stephanie Cohen, and Nana Nikolaishvili-Feinberg in the UNC Translational Pathology Laboratory for the IHC staining and data analysis. We thank Charlene Santos and colleagues in the UNC Animal Studies Core for help with animal studies. This research is based in part upon work conducted using the UNC Proteomics Core Facility, which is supported in part by P30 CA016086 Cancer Center Core Support Grant to the UNC Lineberger Comprehensive Cancer Center.

The costs of publication of this article were defrayed in part by the payment of page charges. This article must therefore be hereby marked *advertisement* in accordance with 18 U.S.C. Section 1734 solely to indicate this fact.

Received March 9, 2020; revised June 15, 2020; accepted July 15, 2020; published first July 20, 2020.

REFERENCES

1. Anders CK, Carey LA. Biology, metastatic patterns, and treatment of patients with triple-negative breast cancer. Clin Breast Cancer 2009;9Suppl 2:S73–81.
2. Metzger O, Tutt A, de Azambuja E, Saini KS, Viale G, Loi S, et al. Dissecting the heterogeneity of triple-negative breast cancer. J Clin Oncol 2012;30:1879–87.
3. Wahba HA, El-Hadaad HA. Current approaches in treatment of triple-negative breast cancer. Cancer Biol Med 2015;12:106–16.
4. Losman JA, Kaelin WG Jr. What a difference a hydroxyl makes: mutant IDH, (R)-2-hydroxyglutarate, and cancer. Genes Dev 2013;27:836–52.
5. Zheng X, Zhai B, Koivunen P, Shin SJ, Lu G, Liu J, et al. Prolyl hydroxylation by EglN2 destabilizes FOXO3a by blocking its interaction with the USP9x deubiquitinase. Genes Dev 2014;28:1429–44.
6. Kaelin WG Jr., Ratcliffe PJ. Oxygen sensing by metazoans: the central role of the HIF hydroxylase pathway. Mol Cell 2008;30:393–402.
7. Cloos PA, Christensen J, Agger K, Helin K. Erasing the methyl mark: histone demethylases at the center of cellular differentiation and disease. Genes Dev 2008;22:1115–40.
8. Varier RA, Timmers HT. Histone lysine methylation and demethylation pathways in cancer. Biochim Biophys Acta 2011;1815:75–89.
9. Takada M, Zhuang M, Inuzuka H, Zhang J, Zurlo G, Zhang JF, et al. EglN2 contributes to triple negative breast tumorigenesis by functioning as a substrate for the FBW7 tumor suppressor. Oncotarget 2017;8:6787–95.
10. Zurlo G, Liu XJ, Takada M, Fan C, Simon JM, Ptacek TS, et al. Prolyl hydroxylase substrate adenylosuccinate lyase is an oncogenic driver in triple negative breast cancer. Nat Commun 2019;10:5177.
11. Paul HS, Sekas G, Adibi SA. Carnitine biosynthesis in hepatic peroxisomes. Demonstration of gamma-butyrobetaine hydroxylase activity. Eur J Biochem 1992;203:599–605.
12. Kim JH, Sharma A, Dhar SS, Lee SH, Gu B, Chan CH, et al. UTX and MLL4 coordinately regulate transcriptional programs for cell proliferation and invasiveness in breast cancer cells. Cancer Res 2014;74:1705–17.
13. Lee YF, Miller LD, Chan XB, Black MA, Pang B, Ong CW, et al. JMJD6 is a driver of cellular proliferation and motility and a marker of poor prognosis in breast cancer. Breast Cancer Res 2012;14:R85.
14. Cancer Genome Atlas Network. Comprehensive molecular portraits of human breast tumours. Nature 2012;490:61–70.

15. Curtis C, Shah SP, Chin SF, Turashvili G, Rueda OM, Dunning MJ, et al. The genomic and transcriptomic architecture of 2,000 breast tumours reveals novel subgroups. Nature 2012;486:346–52.
16. Prat A, Parker JS, Karginova O, Fan C, Livasy C, Herschkowitz JI, et al. Phenotypic and molecular characterization of the claudin-low intrinsic subtype of breast cancer. Breast Cancer Res 2010;12:R68.
17. Badve S, Dabbs DJ, Schnitt SJ, Baehner FL, Decker T, Eusebi V, et al. Basal-like and triple-negative breast cancers: a critical review with an emphasis on the implications for pathologists and oncologists. Mod Pathol 2011;24:157–67.
18. Leung IK, Krojer TJ, Kochan GT, Henry L, von Delft F, Claridge TD, et al. Structural and mechanistic studies on gamma-butyrobetaine hydroxylase. Chem Biol 2010;17:1316–24.
19. Vaz FM, van Gool S, Ofman R, Ijlst L, Wanders RJ. Carnitine biosynthesis: identification of the cDNA encoding human gamma-butyrobetaine hydroxylase. Biochem Biophys Res Commun 1998;250:506–10.
20. Bremer J. Carnitine–metabolism and functions. Physiol Rev 1983;63:1420–80.
21. Chong J, Wishart DS, Xia J. Using metaboanalyst 4.0 for comprehensive and integrative metabolomics data analysis. Curr Protoc Bioinformatics 2019;68:e86.
22. Rizzuto R, Marchi S, Bonora M, Aguiari P, Bononi A, De Stefani D, et al. Ca2+ transfer from the ER to mitochondria: when, how and why. Biochim Biophys Acta 2009;1787:1342–51.
23. Shibao K, Fiedler MJ, Nagata J, Minagawa N, Hirata K, Nakayama Y, et al. The type III inositol 1,4,5-trisphosphate receptor is associated with aggressiveness of colorectal carcinoma. Cell Calcium 2010;48:315–23.
24. Kang SS, Han KS, Ku BM, Lee YK, Hong J, Shin HY, et al. Caffeine-mediated inhibition of calcium release channel inositol 1,4,5-trisphosphate receptor subtype 3 blocks glioblastoma invasion and extends survival. Cancer Res 2010;70:1173–83.
25. Mound A, Rodat-Despoix L, Bougarn S, Ouadid-Ahidouch H, Matifat F. Molecular interaction and functional coupling between type 3 inositol 1,4,5-trisphosphate receptor and BKCa channel stimulate breast cancer cell proliferation. Eur J Cancer 2013;49:3738–51.
26. Rezuchova I, Hudecova S, Soltysova A, Matuskova M, Durinikova E, Chovancova B, et al. Type 3 inositol 1,4,5-trisphosphate receptor has antiapoptotic and proliferative role in cancer cells. Cell Death Dis 2019; 10:186.
27. Kuchay S, Giorgi C, Simoneschi D, Pagan J, Missiroli S, Saraf A, et al. PTEN counteracts FBXL2 to promote IP3R3- and Ca(2+)-mediated apoptosis limiting tumour growth. Nature 2017;546:554–8.
28. Emanuele MJ, Elia AE, Xu Q, Thoma CR, Izhar L, Leng Y, et al. Global identification of modular cullin-RING ligase substrates. Cell 2011;147:459–74.
29. Detre S, Saclani Jotti G, Dowsett M. A "quickscore" method for immunohistochemical semiquantitation: validation for oestrogen receptor in breast carcinomas. J Clin Pathol 1995;48:876–8.
30. Cardenas C, Miller RA, Smith I, Bui T, Molgo J, Muller M, et al. Essential regulation of cell bioenergetics by constitutive InsP3 receptor Ca2+ transfer to mitochondria. Cell 2010;142:270–83.
31. Mound A, Vautrin-Glabik A, Foulon A, Botia B, Hague F, Parys JB, et al. Downregulation of type 3 inositol (1,4,5)-trisphosphate receptor decreases breast cancer cell migration through an oscillatory Ca2+ signal. Oncotarget 2017;8:72324–41.
32. Liberti MV, Locasale JW. The warburg effect: how does it benefit cancer cells? (vol 41, pg 211, 2016). Trends Biochem Sci 2016;41:287.
33. Brown KK, Spinelli JB, Asara JM, Toker A. Adaptive reprogramming of de novo pyrimidine synthesis is a metabolic vulnerability in triple-negative breast cancer. Cancer Discov 2017;7:782.
34. Laplante M, Sabatini DM. mTOR signaling in growth control and disease. Cell 2012;149:274–93.
35. Ben-Sahra I, Manning BD. mTORC1 signaling and the metabolic control of cell growth. Curr Opin Cell Biol 2017;45:72–82.
36. Gulati P, Gaspers LD, Dann SG, Joaquin M, Nobukuni T, Natt F, et al. Amino acids activate mTOR complex 1 via Ca2+/CaM signaling to hVps34. Cell Metab 2008;7:456–65.
37. Mercan F, Lee H, Kolli S, Bennett AM. Novel role for SHP-2 in nutrient-responsive control of S6 kinase 1 signaling. Mol Cell Biol 2013;33:293–306.
38. Li RJ, Xu J, Fu C, Zhang J, Zheng YG, Jia H, et al. Regulation of mTORC1 by lysosomal calcium and calmodulin. Elife 2016;5:e19360.
39. Thastrup O, Cullen PJ, Drobak BK, Hanley MR, Dawson AP. Thapsigargin, a tumor promoter, discharges intracellular Ca2+ stores by specific inhibition of the endoplasmic reticulum Ca2(+)-ATPase. Proc Natl Acad Sci U S A 1990;87:2466–70.
40. Simkhovich BZ, Shutenko ZV, Meirena DV, Khagi KB, Mezapuke RJ, Molodchina TN, et al. 3-(2,2,2-Trimethylhydrazinium)propionate (THP)–a novel gamma-butyrobetaine hydroxylase inhibitor with cardioprotective properties. Biochem Pharmacol 1988;37:195–202.
41. Tars K, Leitans J, Kazaks A, Zelencova D, Liepinsh E, Kuka J, et al. Targeting carnitine biosynthesis: discovery of new inhibitors against gamma-butyrobetaine hydroxylase. J Med Chem 2014;57:2213–36.
42. Rydzik AM, Chowdhury R, Kochan GT, Williams ST, McDonough MA, Kawamura A, et al. Modulating carnitine levels by targeting its biosynthesis pathway - selective inhibition of gamma-butyrobetaine hydroxylase. Chem Sci 2014;5:1765–71.
43. Bianchini G, Balko JM, Mayer IA, Sanders ME, Gianni L. Triple-negative breast cancer: challenges and opportunities of a heterogeneous disease. Nat Rev Clin Oncol 2016;13:674–90.
44. Ivan M, Kondo K, Yang H, Kim W, Valiando J, Ohh M, et al. HIFalpha targeted for VHL-mediated destruction by proline hydroxylation: implications for O2 sensing. Science 2001;292:464–8.
45. Chan MC, Holt-Martyn JP, Schofield CJ, Ratcliffe PJ. Pharmacological targeting of the HIF hydroxylases–A new field in medicine development. Mol Aspects Med 2016;47–48:54–75.
46. Clapham DE. Calcium signaling. Cell 2007;131:1047–58.
47. Roderick HL, Cook SJ. Ca2+ signalling checkpoints in cancer: remodelling Ca2+ for cancer cell proliferation and survival. Nat Rev Cancer 2008;8:361–75.
48. Monteith GR, Prevarskaya N, Roberts-Thomson SJ. The calcium-cancer signalling nexus. Nat Rev Cancer 2017;17:367–80.
49. Foskett JK, White C, Cheung KH, Mak DO. Inositol trisphosphate receptor Ca2+ release channels. Physiol Rev 2007;87:593–658.
50. Mangla A, Guerra MT, Nathanson MH. Type 3 inositol 1,4,5-trisphosphate receptor: A calcium channel for all seasons. Cell Calcium 2020;85:102132.
51. Szatkowski C, Parys JB, Ouadid-Ahidouch H, Matifat F. Inositol 1,4,5-trisphosphate-induced Ca2+ signalling is involved in estradiol-induced breast cancer epithelial cell growth. Mol Cancer 2010;9:156.
52. Cui C, Merritt R, Fu L, Pan Z. Targeting calcium signaling in cancer therapy. Acta Pharm Sin B 2017;7:3–17.
53. Zhu Y, Zhang GY, Zhao J, Li DS, Yan XD, Liu JF, et al. Efficacy and safety of mildronate for acute ischemic stroke: a randomized, double-blind, active-controlled phase ii multicenter trial. Clin Drug Invest 2013;33:755–60.
54. Dzerve V, Group MIS. A dose-dependent improvement in exercise tolerance in patients with stable angina treated with mildronate: a clinical trial "MILSS I." Medicina 2011;47:544–51.
55. Spaniol M, Brooks H, Auer L, Zimmermann A, Solioz M, Stieger B, et al. Development and characterization of an animal model of carnitine deficiency. Eur J Biochem 2001;268:1876–87.
56. Liepinsh E, Dambrova M. The unusual pharmacokinetics of meldonium: Implications for doping. Pharmacol Res 2016;111:100.
57. Degrace P, Demizieux L, Du ZY, Gresti J, Caverot L, Djaouti L, et al. Regulation of lipid flux between liver and adipose tissue during transient hepatic steatosis in carnitine-depleted rats. J Biol Chem 2007;282:20816–26.
58. Fink MA, Paland H, Herzog S, Grube M, Vogelgesang S, Weitmann K, et al. L-carnitine-mediated tumor cell protection and poor patient survival associated with OCTN2 overexpression in glioblastoma multiforme. Clin Cancer Res 2019;25:2874–86.
59. Liu XJ, Simon JM, Xie HB, Hu LX, Wang J, Zurlo G, et al. Genome-wide screening identifies SFMBT1 as an oncogenic driver in cancer with VHL loss. Mol Cell 2020;77:1294–306.
60. Hu LX, Xie HB, Liu XJ, Potjewyd F, James LI, Wilkerson EM, et al. TBK1 is a synthetic lethal target in cancer with VHL loss. Cancer Discov 2020;10:460–75.

Published OnlineFirst July 20, 2020; DOI: 10.1158/2159-8290.CD-20-0288

AACR American Association for Cancer Research

CANCER DISCOVERY

Identification of BBOX1 as a Therapeutic Target in Triple-Negative Breast Cancer

Chengheng Liao, Yang Zhang, Cheng Fan, et al.

Cancer Discov Published OnlineFirst July 20, 2020.